American Mineralogist, Volume 81, pages 706–718, 1996

Diffusion of the hydrous component in pyrope

LIPING WANG, YOUXUE ZHANG,* AND ERIC J. ESSENE

Department of Geological Sciences, University of Michigan, Ann Arbor, Michigan 48109-1063, U.S.A.

ABSTRACT

Dehydrogenation experiments have been performed on natural pyrope megacrysts ($Py_{70}Alm_{16}Gr_{14}$) containing 22–112 ppm total H_2O by weight (H/Si is from 0.00035 to 0.0018). The concentrations of OH in pyrope crystals were determined by Fourier-transform infrared spectroscopy. Two methods were used to obtain diffusivities. One method involved measurement of OH concentration profiles after a heating experiment. The diffusivity of the hydrous component was found to be proportional to the OH concentration along each profile, indicating that the diffusing species is not OH and is probably a minor or trace species with a concentration proportional to the square of the OH concentration (such as H_2). Hence, the diffusivities are referred to as the apparent diffusivities (D^*, which equals D_0^*C/C_0, where C_0 is the initial OH concentration and D_0^* is the D^* when $C = C_0$). The other method involved measurement of the overall decrease of OH content across a wafer as a function of cumulative heating duration. From the overall decrease of OH content, the apparent bulk diffusion-out diffusivities ($\overline{D_{out}^*}$) were obtained. ($\overline{D_{out}^*}$, $\overline{D_{in}^*}$, and D_0^* are different if D^* depends on concentration.) The diffusivities from the two methods are consistent for a given pyrope crystal. However, the $\overline{D_{out}^*}$ values in different pyrope crystals are roughly inversely proportional to the initial OH content in the crystal, opposite the concentration dependence of D^* along a diffusion profile. This apparent paradox places strong constraints on the diffusion and incorporation mechanism of the hydrous component in pyrope and indicates a control on the concentration of the diffusing species by factors other than OH content (such as Fe^{3+}/Fe^{2+}). Any proposed diffusion mechanism must be able to explain this apparent paradox (both the proportionality and the inverse proportionality).

The $\overline{D_{out}^*}$ values (in squared micrometers per second) in a crystal with 82–90 ppm initial total H_2O can be described by $\ln \overline{D_{out}^*} = [(28.20 \pm 1.30) - (30580 \pm 1450)]/T$ (where T is temperature in kelvins and errors are at the 2σ level). The $\overline{D_{out}^*}$ values are greater by a factor of ~3 in a crystal with 22–23 ppm initial total H_2O. The D_0^* values can be determined by dividing the $\overline{D_{out}^*}$ values by 0.347, and D^* at each concentration can be determined from $D^* = D_0^*C/C_0$. The average activation energy for hydrous component diffusion in the two crystals is 253 ± 13 (2σ) kJ/mol. The diffusion-out diffusivities of the hydrous component are seven to eight orders of magnitude greater than the Fe-Mg interdiffusivities. They are so large that the OH content of a pyrope crystal can adjust to changing environmental conditions on a time scale of hours at temperatures as low as 800 °C. Pyrope crystals from the mantle may dehydrogenate during ascent. Caution should be exercised in using OH content in natural pyrope crystals to infer conditions of the source region.

INTRODUCTION

Mantle-derived, nominally anhydrous pyrope often contains a structurally bonded hydrous component. Aines and Rossman (1984a, 1984b) and Bell and Rossman (1992a) made a systematic infrared (IR) study of OH in mantle-derived garnet and found that garnet typically contained a major band at 3570 cm^{-1} and a smaller band at 3670 cm^{-1}. There may also be a shoulder on the 3570 cm^{-1} band. When the 3570 cm^{-1} band is small, the shoulder band appears as a distinct band centered at 3512 cm^{-1}. Although OH is the only species measurable by IR, the concentration of OH is often expressed as weight in parts per million H_2O (referred to as H_2O_{tot} hereafter) that ranges from nearly zero to several hundred parts per million (e.g., Bell and Rossman 1992b). Garnet is a major mineral in the mantle with a volume fraction approaching 40% in the transition zone owing to the dissolution of pyroxene into garnet (e.g., Ringwood 1991). Therefore, the presence of trace amounts of hydrous component in garnet (and other nominally anhydrous minerals) has generated considerable interest because it may serve as a repository for H_2O in the mantle and affect the melting point and rheology of the mantle (e.g., Wyllie 1979;

*Author to whom all correspondence should be addressed.

0003-004X/96/0506-0706$05.00

TABLE 1. Composition of starting pyrope crystals

Sample	Py-1	Py-4	Py-6	Py-7	Py-23	Py-24	AZPy-1	MSPy-1	GR-2	GR-3	GR-5
Source	a	a	a	a	a	a	b	c	d	d	d
SiO_2	41.47	42.09	41.73	42.07	42.31	41.84	42.36	42.36	42.94	41.34	42.40
TiO_2	0.09	0.08	0.11	0.09	0.10	0.07	0.07	0.12	0.14	0.07	0.02
Al_2O_3	22.01	22.34	21.00	22.59	22.30	22.05	21.00	22.25	22.73	23.81	21.05
Cr_2O_3	1.99	1.95	3.77	2.07	1.94	2.26	4.06	2.09	1.69	0.29	3.64
FeO	8.96	8.30	7.97	8.33	8.06	7.98	7.63	7.23	8.55	10.59	8.09
MnO	0.42	0.32	0.36	0.42	0.33	0.34	0.50	0.28	0.42	0.42	0.52
MgO	18.96	19.62	19.93	18.88	19.13	19.46	19.25	20.31	18.71	19.45	19.20
CaO	5.44	5.39	4.97	5.52	5.40	5.64	5.16	5.39	5.33	4.19	5.44
Total	99.34	100.1	99.84	99.97	99.57	99.64	100.0	100.0	100.5	100.2	100.4
H_2O (ppm)*	82–90	22–23	92–112	59–62	22–23	30–33	104–108	38–40	38–61	62–116	32–44
Gr (%)	13.9	13.7	12.7	14.3	14.0	14.4	13.5	13.6	13.9	10.5	14.0
Alm (%)	17.9	16.4	15.9	16.8	16.3	15.9	15.6	14.3	17.4	20.7	16.2
Py (%)	67.4	69.3	70.7	68.0	69.0	69.1	69.9	71.5	67.8	67.9	68.7
Color	red	purple	red	red	purple	red	red	red	red	orange	purple
Comments**	2	2	1	2	3	2	1	1	2,3	2,4	1

Note: All Fe expressed as FeO and oxides as weight percent. Sources are as follows: a = G.E. Harlow of American Museum of Natural History in New York (catalog no. 29423); b = mineral collections of the Department of Geological Sciences, University of Michigan; c = Moses Rock diatreme, Utah; d = Garnet Ridge diatreme, Arizona.

* OH content away from the rim expressed as ppm total H_2O by weight, determined by Fourier-transform IR spectroscopy using the calibration of Bell et al. (1995).

** 1 = no visible inclusions, 2 = acicular rutile inclusions, 3 = small olivine, 4 = rodlike rutile.

Mackwell et al. 1985; Jackson and Pollack 1987; Bell and Rossman 1992a, 1992b; Bell 1993).

The H_2O content of pyrope has been found to vary with factors such as tectonic setting, crystallization history, and host-rock type (Bell and Rossman 1992a). However, the possible loss or gain of OH during the transport of garnet from the source region to the surface has not been fully addressed. To address the problem of whether OH concentrations in mantle-derived garnets represent those in the source region, Bell (1993) experimentally examined the behavior of OH in garnet upon heating to 500–1000 °C. Although rapid loss of the hydrous component was indicated, no quantitative information on diffusivities was obtained.

A quantitative understanding of the diffusion rate of the hydrous component into and out of pyrope is essential to answer questions such as whether the H_2O content of mantle-derived minerals represents that in the source region. Furthermore, diffusion data may allow an inference of diffusion mechanism and species (Doremus 1969; Zhang et al. 1991a, 1991b), which in turn may provide clues to the incorporation mechanism of the hydrous component in garnet. Diffusion of the hydrous component in garnet may also be used, in theory, as a geospeedometer to determine the ascent rate. In this paper, we report an experimental study expanding on the work of Bell (1993) to determine the diffusion rate of hydrous component out of mantle-derived pyrope crystals.

EXPERIMENTAL AND ANALYTICAL METHODS

Starting materials

The megacrysts of pyrope (typically $Py_{70}Alm_{16}Gr_{14}$) used in this study came from ultramafic diatremes of the Colorado Plateau. Table 1 lists the compositions and sources of the crystals used in this study. The initial H_2O_{tot} concentration ranged from 22 to 112 ppm (H/Si is from 0.00035 to 0.0018) (Table 1), as determined by IR spectra (two spectra are shown in Fig. 1). The pyrope megacrysts were roughly equidimensional with diameters from ~5 to ~10 mm. Each crystal was ground with silicon carbide strips, polished with 0.3 μm alumina powder to obtain two parallel surfaces, and then examined for inclusions and cracks using an optical microscope. Although inclusions and cracks were often present, the chosen starting pieces were crack free and almost inclusion free. Most of the garnet crystals we examined, including those used as starting material for our experiments, contained acicular rutile inclusions. These rutile inclusions were typically ~1 μm in diameter and 100–200 μm apart from one another, but some needles might extend across the whole garnet crystal. The rutile inclusions did not have a significant effect on the IR spectra of pyrope, as shown by the absence of the typical OH bands of rutile (Rossman

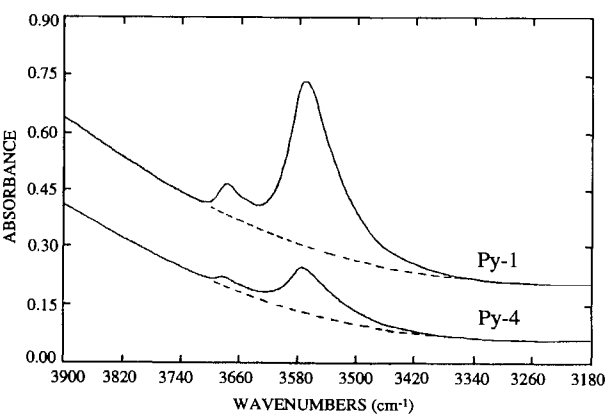

FIGURE 1. Typical IR spectra of starting garnet crystals. Sample thickness: 3.890 mm for Py-1 and 3.470 mm for Py-4. The dashed curves are polynomial fits to the estimated baselines.

TABLE 2. Experimental conditions and diffusivities

Sample	Atm	T (°C)	Point	Thickness (mm)	Cumulative duration (s)	$\overline{D^*_{out}}$ ($\mu m^2/s$)†	$\overline{D^*_{out}}$ ($\mu m^2/s$)‡
Py-1e	air	800	1	1.636	187 740	0.78(0.03)§	0.70(0.03)
	air	800	2	1.638	119 340	0.69(0.04)	0.63(0.03)
	air	800	3	1.622	119 340	0.74(0.07)	0.66(0.05)
Py-1g	air	850	1	1.598	33 600	3.11(0.20)	2.91(0.14)
	air	850	2	1.593	33 600	3.37(0.30)	3.02(0.34)
Py-1f	air	900	1	1.650	9 900	8.5(0.5)	9.4(0.5)
	air	900	2	1.652	8 100	12.0(2.3)	11.0(1.9)
	air	900	3	1.647	6 900	12.5(4.7)	12.5(4.4)
Py-1b	air	950	1	1.538	4 683	20.5(1.1)	25.2(4.3)
	air	950	2	1.537	2 220	20.6(2.5)	27.1(8.2)
Py-1d	N_2	850	1	1.515	25 800	2.91(0.29)	2.66(0.19)
Py-6a	air	900	1	1.548	10 385	8.1(0.5)	9.8(1.1)
Py-6b	N_2	940	1	0.760	1 380	20.1(0.5)	20.4(2.1)
AZPy-1	air	850	1	2.626	10 830	3.26(1.15)	3.15(0.71)
	air	850	2	2.633	10 830	3.19(1.30)	3.26(0.67)
	air	850	profile	2.633	10 830	—	2.54(0.28)
MSPy-1	air	795	1	3.126	10 200	1.70(0.13)	1.63(0.27)
	air	795	profile	3.126	10 200	—	1.55(0.03)
Py-7a	air	850	1	1.326	23 700	3.17(0.30)	2.96(0.23)
Py-7c	N_2	692	1	0.545	800(h)	—	0.032(.001)
Py-4a	air	850	1	1.763	13 020	9.0(0.8)	7.3(0.5)
	air	850	2	1.755	16 620	9.6(0.4)	7.7(0.6)
Py-4b	N_2	940	1	1.097	1 020	69(10)	53(7)
Py-4d	air	795	1	0.741	6 505	2.52(0.30)	2.30(0.47)
Py-23	air	850	1	2.699	5 710	7.2(0.6)	8.4(0.6)
	air	850	profile	2.699	5 710	—	5.93(1.0)
Py-24	air	795	1	2.724	10 200	3.84(0.84)	3.70(0.31)
	air	795	profile	2.724	10 200	—	3.60(0.12)

† Apparent diffusivity determined from integrated absorbance.
‡ Apparent diffusivity determined from linear absorbance.
§ All errors in parentheses are at the 2σ level.

and Smyth 1990) in the IR spectra of pyrope (Fig. 1) and by the presence of typical OH bands of rutile when a large rutile inclusion was intentionally included in the measured area. The almost inclusion-free interior parts were prepared into wafers with a typical thickness of about 1.5 mm for dehydrogenation experiments. The thickness of the sample was measured with a digital micrometer to a precision of ~ 2 μm. The other dimensions of the polished wafers were usually >3 mm, so they can be treated as infinite for diffusion studies (the diffusion distance is usually <0.7 mm). Each experimental wafer is a small interior piece of a large pyrope megacryst and is uniform in OH content within 4% (2σ error hereafter) relative, except for Py-1 and Py-6 (up to 9% relative). Larger wafers were used for diffusion-profile measurements. The more heterogeneous Py-1 and Py-6 were not used in these profiling experiments. Each pyrope crystal was analyzed for major and minor elements by use of a Cameca electron microprobe with a focused beam of 15 kV and 10 nA using a mixture of synthetic and natural standards (Table 1).

Diffusion experiments

Experiments were conducted by holding doubly polished pyrope wafers in air or in a continuous flow of N_2 at 1 atm total pressure and 692–950 °C, then cooling them in air. The pyrope wafers were not quenched in water because that would have severely cracked the wafers. Two horizontal tube furnaces were used in the heating experiments. Each furnace was equipped with an automatic temperature controller and lined with a silica glass tube through which dry N_2 gas was passed during the experiment. The controlling thermocouple (Platinel-II: Pt35%Au65%/Pt17%Pd83%) was outside the silica tube, and a second thermocouple (type K: Ni90%Al10%/Ni96%Al2%Mn2% or type S: Pt/Pt90%Rh10%) was inside the silica tube to indicate the experimental temperature. The inside thermocouple was calibrated against either the melting point of gold or a thermocouple that had already been calibrated. The accuracy of the reported temperature is usually ± 2 °C, but it is ± 4 °C for samples Py-1f, Py-4d, Py-24, and MSPy-1 because of the deterioration of the type-K thermocouple. When a sample was placed in the hot spot in contact with the tip of the inside thermocouple, the temperature reading from the inside thermocouple initially decreased by up to 20 °C, but a steady temperature was reached in <1 min. The temperature fluctuations over the course of the experiments were ± 1 °C.

Two types of experiments were conducted. Profiling experiments were used to examine the potential concentration dependence of diffusivities of the hydrous component. Mass-loss experiments, which are analytically less demanding, were used to obtain diffusivities at different temperatures. All experimental conditions are listed in Table 2, and details are presented below.

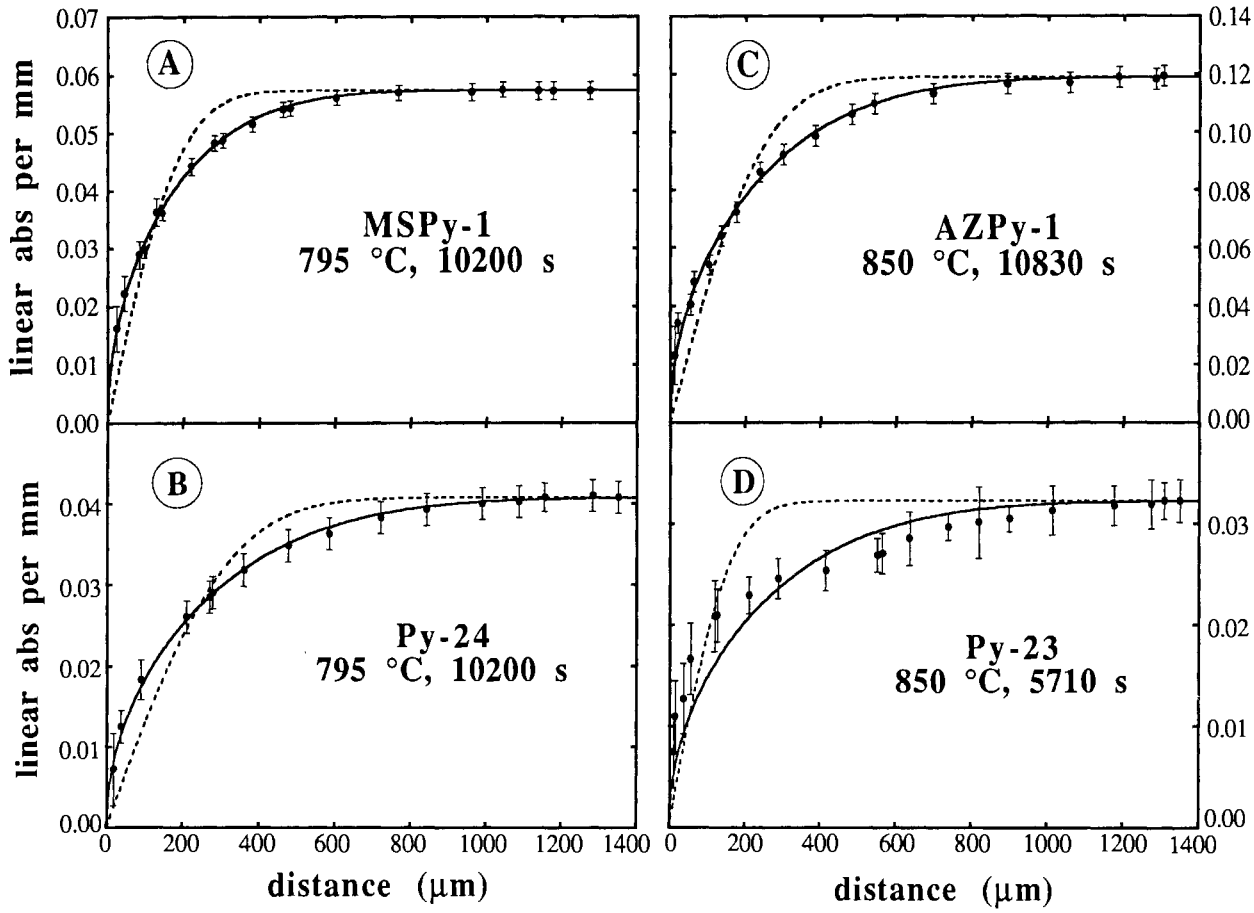

FIGURE 2. Measured OH concentration (in terms of linear absorbance of the major band per millimeter of sample thickness) vs. distance away from the diffusion surface for four garnet crystals. See Table 2 for experimental conditions. The dots are experimental data. The solid curves are the least-squares fits to the data assuming the diffusivity is proportional to OH concentration, and the dashed curves are the least-squares fits assuming constant diffusivity along each profile.

Profiling experiments. The procedure of dehydrogenation experiments to measure diffusion profiles generally followed that of Zhang et al. (1991a). A doubly polished wafer was partially dehydrogenated in a horizontal furnace at a specified temperature and for a certain duration of time, which was long enough to generate a profile that could be conveniently measured by IR spectroscopy but short enough so that the OH content at the center of the wafer was not changed by diffusion (Fig. 2). After quenching, the wafer was sectioned perpendicular to its polished surfaces near its center. This provided a pyrope slice with a complete diffusion profile. The slice was then polished on both sides with a final thickness of ≤ 1 mm and analyzed for the OH concentration profile by IR. Diffusivities were obtained by fitting the profiles. Four profiles were obtained (Fig. 2).

It is possible that during heating a significant amount of OH converts into another H species that is invisible to IR (D.R. Bell, personal communication). This possibility is worth examining because such a conversion would invalidate reported measurements of OH and calibrations in pyrope (Bell and Rossman 1992a, 1992b; Bell et al. 1995) because every natural pyrope crystal has experienced an unknown thermal history. If such a reaction operated alone without diffusion, it would lower the OH concentration uniformly across the profile (that is, the OH concentration would be a constant). If such a reaction modified OH concentration significantly, simultaneously with diffusion, it would lower the OH concentration measurably at the center of the profile. The observations that (1) the OH concentration is not constant and depends on the distance away from the diffusion surface, (2) the OH concentration approaches zero as the surface is approached, and (3) the OH concentration far away from the diffusion surface is the same as the initial concentration, demonstrate that the decrease of OH concentration is due to diffusion out of pyrope, and not the result of a homogeneous reaction that converts OH into H species that are invisible to IR. The concentration of other H species (such as molecular H_2) that may interconvert with OH must be negligible in comparison with that of OH. Hence, measured concentrations of OH (and average

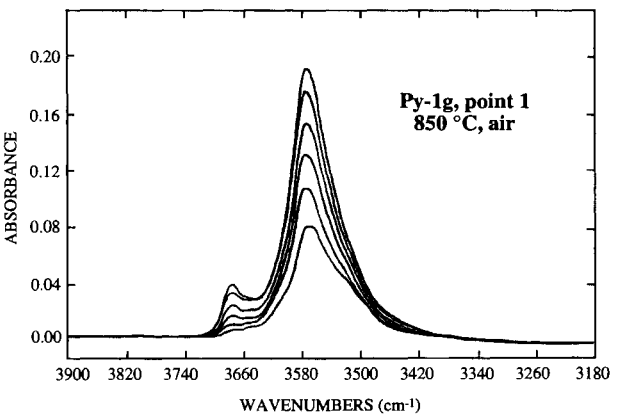

FIGURE 3. A representative series of baseline-subtracted spectra of point 1, Py-1g upon heating in air at 850 °C. The cumulative heating durations are 0.00, 0.33, 2.00, 5.00, 9.30, and 15.0 h for spectra from top to bottom.

concentrations in the mass-loss experiments) are unaffected by possible interconversion of H species.

Mass-loss experiments. The procedure of using mass-loss dehydrogenation experiments to study the diffusion of the hydrous component generally followed that of Jambon et al. (1992), except that we determined the remaining OH content in a garnet wafer by IR spectroscopy, whereas Jambon et al. (1992) determined the H_2O mass loss by weighing the whole experimental charge with a microbalance. Each wafer was heated under the same conditions for 5–15 successive periods, with each period ranging from 2 min to 14 d. After each heating step, the remaining OH content across the whole wafer was measured by IR without repolishing. The difference between the initial and the remaining OH content measured at the same point is the mass loss at that point during the cumulative heating period. All the successive heating steps of the same wafer under the same conditions are referred to as a series of experiments. All spectra before and after such heating steps are called a series of spectra (Fig. 3). Heating experiments were conducted on wafers from eight garnet crystals with various initial OH concentrations.

After each heating step, the garnet wafer was reexamined optically. Cracked samples were discarded. In heating experiments in air at 900–950 °C, the surfaces of the wafers were slightly oxidized. We believe that the very thin oxidized layer did not perturb our results because the diffusion distance is much greater than the thickness of the oxidized layer and because the IR spectra did not show any unusual aspect. The wafer Py-1f was examined by TEM after it was heated in air at 900 °C for 27 h. It was polished to a thickness of ~40 μm and then ion milled to obtain a thinned area of about 15000 μm^2 around a hole. TEM analysis revealed no microcracks or decomposition inside the pyrope crystal.

Infrared analysis

The OH content was determined from IR spectra obtained on a Nicolet 60SX FTIR at the University of Michigan following the procedure of Bell and Rossman (1992a). Typical spectra (Fig. 1) in the wavenumber region of interest contained a major band near 3570 cm^{-1} and a minor band near 3670 cm^{-1}, superimposed on a broad spin-allowed electronic transition of Fe^{2+} (Rossman 1988). Both major and minor bands are due to structurally bonded OH (Wilkins and Sabine 1973; Aines and Rossman 1984a, 1984b). An additional band at 3512 cm^{-1} (Bell and Rossman 1992a) may be present as a shoulder of the 3570 cm^{-1} band. After the wafer was nearly completely dehydrogenated the 3512 cm^{-1} band became a separate band (Fig. 3). This observation suggests that this band is more immobile than the other OH bands (Bell 1993). On the basis of our direct measurement and calculations using the TiO_2 content vs. band intensity (Bell 1993), the intensity of this band is estimated to be <7% of the major band at 3570 cm^{-1} in the unheated crystals. Therefore, the presence of this band does not affect our results significantly.

The baseline of a spectrum was fitted by a polynomial, and the quality of the fit was always visually checked to ensure that there was no systematic misfit. The baseline shape from the fits was the same as the IR spectrum of a completely dehydrogenated sample. The total area beneath the two bands (the integrated absorbance) was used to estimate the weight in parts per million of H_2O_{tot} calculated as integrated absorbance per centimeter of sample thickness divided by 1.39 (Bell et al. 1995). The peak heights of the two bands at 3570 and 3670 cm^{-1} were also measured. In all experimental cases, the intensity ratio of the minor band to the major band did not change enough to affect the linearity between the intensity of the major band and the integrated absorbance. Therefore, the peak height of the major band at 3570 cm^{-1} is approximately proportional to OH content. Because the peak height can be determined more easily and accurately than the integrated absorbance, it is often used to represent OH concentration.

The precision of the measurement depends on the size of the aperture used to delimit the IR beam, the number of scans, the thickness of the sample, and the OH content of the sample. A round aperture of 510 μm diameter was used for measurements to obtain remaining mass vs. time curves. On the basis of both the quality of the spectra and repeated measurements of a standard using this aperture, the 2σ relative error was ~2% for the linear absorbance and ~3% for the integrated absorbance except for samples with very low absorbance (dehydrogenated samples or thinner samples), for which the 2σ relative error was greater and estimated from the quality of the spectra. These uncertainties are somewhat greater than those for H_2O and OH contents in rhyolitic glasses from this laboratory. The accuracy of the measurements depends on the accuracy of the calibration by Bell et al.

(1995). However, accurate extraction of diffusivities requires only precise OH determination and is independent of the accuracy.

A 10 μm × 1 mm slit was used to measure the diffusion profiles. In profiling, the distance from the edge of the wafer to the center of the slit was determined using an optical microscope with a reading precision of 2 μm. Actual uncertainty in the distance determination was probably ~5 μm because of the width of the beam, the divergence of the beam inside the sample, and the convolution effect. With the 10 μm × 1 mm slit, the 2σ relative error was ~2% for the linear absorbance and ~5% for the integrated absorbance except for samples with very low absorbance, for which the error was greater and therefore estimated from the quality of the spectrum.

Results and discussion

Diffusion profiles

Four diffusion profiles (Fig. 2) were measured to examine the dependence of diffusivities of the hydrous component on OH concentrations in a single pyrope crystal. The OH concentration at the center of each sample remains identical to the initial concentration and decreases toward the rim of the sample in each profile. The smoothness of the profiles shown in Figure 2 (except for Fig. 2D) demonstrates the high quality of our data. The somewhat larger scatter for the profile of Py-23 shown in Figure 2D may be due to the presence of several small inclusions. The profiles were then fitted to theoretical diffusion profiles to obtain diffusivities. When the profiles were fitted by an error function, which is the solution for diffusion with a constant diffusivity, the results were not satisfactory (dashed curves in Fig. 2). Therefore, diffusivity depends on OH concentration. This observation suggests that speciation plays a role in diffusion and that the diffusivity is an apparent diffusivity (Zhang et al. 1991a, 1991b). We therefore used D^* (instead of simple D) to denote the apparent diffusivity of the hydrous component at a given OH content. Furthermore, the steeper slope of the OH concentration relative to that of error function near the surface suggests that the diffusivity decreases with decreasing OH concentration (recall that the diffusivity is inversely proportional to the slope $\partial C/\partial x$ in Boltzmann-Matano analysis). We therefore adopted the approach of Zhang et al. (1991a) and Zhang and Stolper (1991) to fit the profiles by assuming that the diffusivity is proportional to the OH content. That is, the diffusion equation is

$$\frac{\partial C}{\partial t} = \frac{\partial}{\partial x}\left(D^* \frac{\partial C}{\partial x}\right) \tag{1}$$

where the initial condition is $C|_{t=0,\, x\geq 0} = C_0$, the boundary condition is $C|_{x=0,\, t>0} = 0$, and $D^* = D_0^* C/C_0$ (D_0^* is D^* at $C = C_0$). Given the initial concentration, C_0 (the same as the concentration near the center), the diffusion profile is fitted by the solution of Equation 1 to obtain the single unknown D_0^*. The resulting fits (solid curves in Fig. 2) are excellent in three cases (Figs. 2A–2C) and marginal in one case (Fig. 2D), suggesting that the data are consistent with the assumption of the proportionality between D^* and OH concentration. This proportionality suggests that OH is not likely the diffusing species; otherwise, at such low contents, OH diffusion would be similar to tracer diffusion and would have a constant diffusivity. The proportionality means that the diffusive flux is proportional to the gradient of the square of OH concentration [$-J = D^*\partial C/\partial x = (0.5D_0^*/C_0)\partial C^2/\partial x$]. This observation is similar to water diffusion in silica glass (Doremus 1969), rhyolitic glass at $\leq$0.2% H_2O_{tot} (Zhang et al. 1991a; Jambon et al. 1992), and basaltic melt (Zhang and Stolper 1991). The observation is best explained by the diffusion of a species with a concentration that is much lower than the OH concentration and is approximately proportional to the square of the OH concentration (Doremus 1969; Zhang et al. 1991a, 1991b; Zhang and Stolper 1991). Two candidates that satisfy the observation are molecular H_2O and H_2.

Mass-loss experiments

Mass-loss experiments were conducted with wafers from eight pyrope crystals. For each sample, spectra were measured across the whole wafer at approximately the same point before and after each heating step. Measuring the OH content at approximately the same point minimizes the effect of small heterogeneity of the sample on the diffusion data. The absorbance owing to structural OH decreased upon heating, indicating loss of OH. A representative series of spectra upon heating (Py-1g, 850 °C, air) is shown in Figure 3. The remaining OH content across the whole wafer is plotted against the square root of the cumulative heating duration (Fig. 4). The smooth linear trends illustrate the quality of our data.

The apparent diffusivity of the hydrous component diffusing out of garnet is referred to as the diffusion-out diffusivity, $\overline{D_{out}^*}$. If the OH concentration at the center has not been affected by heating, the mass loss is proportional to the square root of time, and the diffusion-out diffusivity can be treated as a constant because the concentration profile propagates into the crystal according to the square root of time, regardless of the concentration dependence of D^*, if the concentration at the center is unchanged (Zhang et al. 1989, 1991a). The diffusion-out diffusivity was obtained from the mass-loss equation from a semi-infinite medium (Eq. 3.15 in Crank 1975) rewritten as

$$M_t = M_0 - M_0 \sqrt{\frac{16\overline{D_{out}^*}}{\pi L^2}}\sqrt{t} \tag{2}$$

where M_0 is the initial OH content across the whole wafer ($M_0 = C_0 L$ with uniform C_0), M_t is the remaining OH content across the whole wafer affected by a diffusion profile, and L is the thickness of the wafer. If diffusivity is independent of concentration, the relative error caused by application of Equation 2 can be obtained by comparing Equation 2 with Equation 4.20 in Crank (1975)

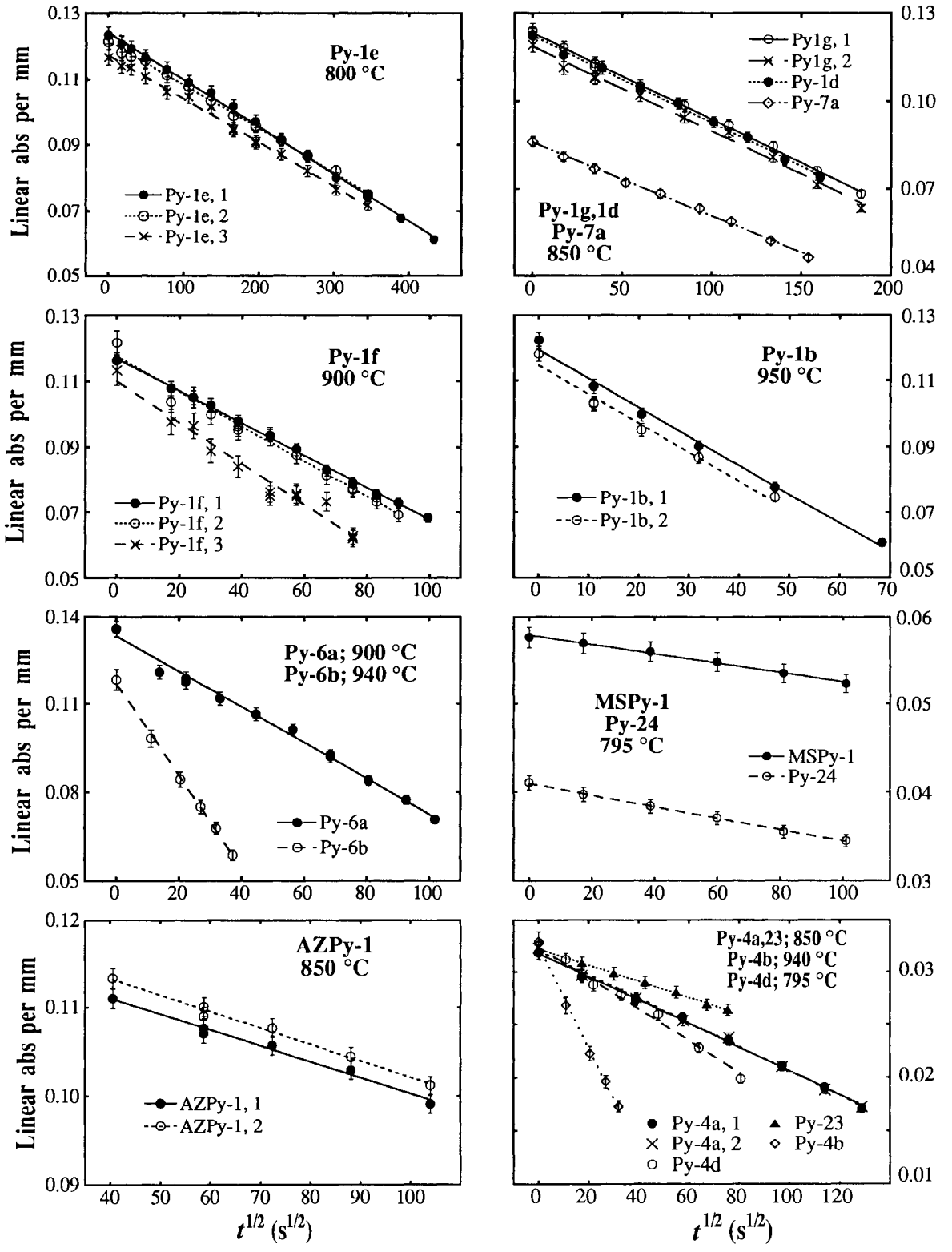

FIGURE 4. Remaining mass of OH in terms of linear absorbance at 3570 cm^{-1} per mm sample thickness vs. the square root of cumulative time. Linear least-squares fits to the data are also shown. Only the data with <50% of mass loss are shown and used in the fits.

(Eq. 5 later), the analytic solution for diffusion in a plane sheet. The relative error is <0.87% if mass loss is <65%. If D^* is proportional to C, Equation 2 holds for mass loss of ≤50% (see Fig. 5 later). By plotting either the linear or integrated absorbance vs. the square root of cumulative time for a given series of experiments with mass loss <50%, $\overline{D^*_{out}}$ may be calculated from the slope and the intercept as $(\pi L^2/16)$(slope/intercept)^2 (Table 2). The uncertainty in $\overline{D^*_{out}}$ was obtained from the uncertainties in the slope and intercept from the fits (the uncertainty in thickness is <0.2% relative and negligible; the uncertainty in time is typically 20 s and is also negligible).

Because of the concentration dependence of D^*, $\overline{D^*_{out}}$ is an average diffusivity over a concentration range of 0 to C_0. The diffusion-out diffusivity is not the same as D^*_0, nor the D^* at the surface where $C = 0$ and $D^* = 0$. Although D^* depends only on the concentration and does not depend on the direction of diffusion, the diffusion-out diffusivity is different from the diffusion-in diffusivity ($\overline{D^*_{in}}$) because of the concentration dependence of D^* (Moulson and Roberts 1961; Zhang et al. 1991a). For example, in the case of $D^* = D^*_0 C/C_0$, it can be shown that $\overline{D^*_{out}}$ is related to D^*_0 (Zhang et al. 1991a) by

$$\overline{D^*_{out}} = 0.347 D^*_0 \quad (3)$$

if $C|_{t=0,\, x\geq 0} = C_0$ and $C|_{x=0,\, t>0} = 0$. The apparent diffusion-in diffusivity is related to D^*_0 as

$$\overline{D^*_{in}} = 0.619 D^*_0 \approx 1.78 \overline{D^*_{out}} \quad (4)$$

if $C|_{t=0,\, x\geq 0} = 0$ and $C|_{x=0,\, t>0} = C_0$. These relationships can be used to relate D^*_0 values obtained from the profiling experiments and $\overline{D^*_{out}}$ values obtained from the mass-loss experiments.

Figure 4 shows the results of all mass-loss experiments for which the mass loss is <50% and Equation 2 is applicable. The linear absorbance across the whole wafer (proportional to M_t) is plotted against $t^{1/2}$. The linear fits of M_t vs. $t^{1/2}$ are also shown. All fits are excellent. From the fits, $\overline{D^*_{out}}$ values with 2σ uncertainties were obtained and are reported in Table 2. Plotting integrated absorbance vs. $t^{1/2}$ gives similar results. The $\overline{D^*_{out}}$ values obtained from the integrated absorbance are also reported in Table 2 and are in excellent agreement with those obtained from the linear absorbance. The tracking of several points in a wafer also yielded $\overline{D^*_{out}}$ values that are in good agreement. The relative 2σ errors for $\overline{D^*_{out}}$ values are generally <10%. Under similar experimental conditions, $\overline{D^*_{out}}$ values for pyrope crystals with similar initial OH contents were reproducible within 20% relative (e.g., Py-1f and Py-6a).

No significant difference in the diffusivity can be discerned within error between experiments conducted in air and those under a flow of N_2. For example, the average $\overline{D^*_{out}}$ is 3.10 $\mu m^2/s$ for Py-1g (850 °C, in air) and 2.79 $\mu m^2/s$ for Py-1d (850 °C, in N_2 flow). These values agree within ~10%. Because the diffusion of hydrous component is much faster than that of O in crystals under dry conditions, it is expected that O does not participate actively in the diffusion process on the experimental time scale (i.e., the O diffusion into garnet crystal is negligible). Therefore, it is concluded that O_2 in air does not play a significant role in the diffusion process.

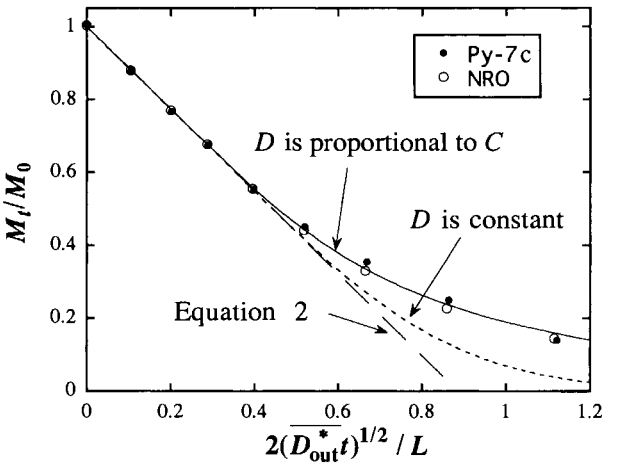

FIGURE 5. Calculated M_t/M_0 vs. $2(\overline{D^*_{out}t})^{1/2}/L$ curves using Equations 2 and 5 (for constant D) and numerical results in the case of D^* proportional to C. Experimental data from Py-7c (solid circles) and a rhyolitic glass (NRO, open circles) are also shown. The $\overline{D^*_{out}}$ values for the two samples were obtained from the first five points. The experimental data are clearly best described by D^* proportional to C.

The $\overline{D^*_{out}}$ values were also obtained from D^*_0 values from the profiling experiments. Using Equation 3, $\overline{D^*_{out}}$ values can be calculated from D^*_0 values of 4.46 ± 0.08, 10.38 ± 0.34, 7.31 ± 0.82, and 17.1 ± 2.87 $\mu m^2/s$, to be 1.55 ± 0.03, 3.60 ± 0.12, 2.54 ± 0.28, and 5.93 ± 1.00 $\mu m^2/s$ for MSPy-1, Py-24, AZPy-1, and Py-23, respectively. These $\overline{D^*_{out}}$ values are also listed in Table 2 and are all in good agreement with those obtained by the mass-loss method. In the worst case (Py-23 at 850 °C in air), $\overline{D^*_{out}}$ from the mass-loss experiment is 8.4 $\mu m^2/s$ and that calculated from D^*_0 from diffusion-profile experiment is 5.9 $\mu m^2/s$. On the basis of all these comparisons, we estimate that on average, the $\overline{D^*_{out}}$ values can be reproduced to within ~20%, somewhat worse than the individual fitting errors of typically 5–10% (Table 2). The smooth concentration profiles and mass-loss trends, and the high reproducibility of diffusivities, all demonstrate the high quality of our diffusion data.

If the concentration at the center is affected by diffusion, Equation 2 no longer holds. For constant diffusivity D, M_t as a function of t can be obtained by rewriting Equation 4.20 in Crank (1975) as

$$M_t = M_0 - M_0\sqrt{\frac{16D}{\pi L^2}}\sqrt{t}\left[1 + 2\sqrt{\pi}\sum_{n=1}^{\infty}(-1)^n \text{ierfc}\frac{nL}{2\sqrt{Dt}}\right]. \quad (5)$$

However, if D^* depends on C, the above expression does not hold, and M_t vs. t follows a different curve. If $D^* =$

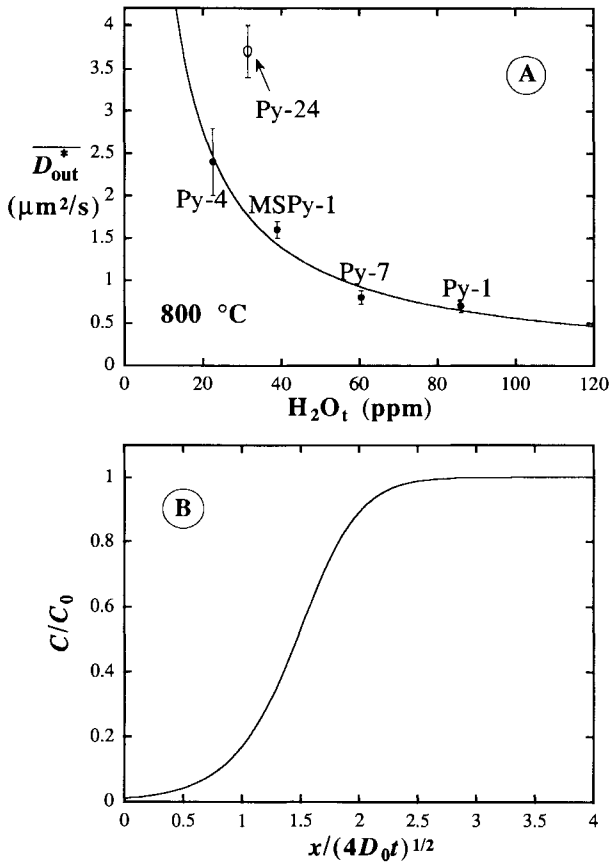

FIGURE 6. (**A**) The $\overline{D^*_{out}}$ values of different pyrope crystals at 800 °C vs. the initial H_2O_{tot} concentration (C_0). The curve is a fit using $\overline{D^*_{out}} = A/C_0$ for Py-1, Py-4, Py-7, and MSPy-1. $\overline{D^*_{out}}$ values for Py-4 and Py-7 were interpolated from experimental data. (**B**) Calculated concentration profile (C vs. x profiles) for $D = D_0C_0/C$ (D inversely proportional to C). The initial condition is $C|_{t=0,\ x\geq 0} = C_0$. The boundary condition is $C|_{x=0,\ t>0} = 0.01C_0$ (a zero boundary condition cannot be applied because D^* would be infinity).

D^*_0C/C_0, as the concentration at the center decreases to less than C_0, D^* at the center becomes less than D^*_0. Hence, the $\overline{D^*_{out}}$ value also decreases because it is the average of the D^* values across the profile. Therefore, for $D^* = D^*_0C/C_0$, the rate of M_t decrease is slower than that predicted by Equation 5. The exact evolution of M_t as a function of t can be numerically calculated by solving the appropriate equation (Zhang et al. 1991a). Figure 5 compares the M_t/M_0 vs. $t^{1/2}$ curve for $D^* = D^*_0C/C_0$, the curve for constant D, and the straight line of Equation 2. The divergence between the curves as M_t/M_0 decreases to <0.4 can clearly be used to determine whether the diffusivity of the hydrous component is constant or is proportional to C.

To confirm further that the apparent diffusivity of the hydrous component is proportional to the OH concentration inferred from diffusion profiles, we conducted a mass-loss experiment (Py-7c, Table 2) at 692 °C under an N_2 flow in which up to 86% of the initial OH was lost by heating. The wafer was 0.545 × 3.1 × 3.5 mm. The length/thickness and width/thickness ratios are large enough that the effect of diffusion from the edges (rather than the two polished surfaces) on OH concentration at the measured point is negligible and one-dimensional diffusion is applicable. A control experiment was conducted simultaneously by dehydrating a rhyolitic glass (NRO, 0.468 × 3.3 × 3.3 mm) with low initial H_2O_{tot} (0.087 wt%). At this low H_2O_{tot}, the apparent H_2O_{tot} diffusivity in rhyolitic glass is proportional to H_2O_{tot} concentration (Zhang et al. 1991a). The resulting data for both the garnet and rhyolitic wafer are plotted on Figure 5. They confirm that the D^* is proportional to H_2O_{tot} for both garnet and the rhyolitic glass. Furthermore, the D^*_0 of the rhyolitic glass at 692 °C (Fig. 5) is 0.0681 $\mu m^2/s$, in excellent agreement with the D^*_0 value of 0.0652 $\mu m^2/s$ calculated using the molecular H_2O diffusivity and the $d[H_2O_m]/d[H_2O_{tot}]$ value from the regular-solution model of Zhang et al. (1991a).

Concentration dependence of the apparent diffusivity of the hydrous component

Diffusion profiles and the mass-loss experiment (Py-7c) show that D^* is proportional to OH concentration in a specific crystal. However, the $\overline{D^*_{out}}$ values of different mantle garnet crystals are roughly inversely proportional to the initial OH content. For example, the initial OH content in Py-1 (~90 ppm H_2O_{tot}) is about 3.8 times that in Py-4 (~23 ppm H_2O_{tot}), but $\overline{D^*_{out}}$ at 800 °C for Py-4 (2.4 $\mu m^2/s$) is about 3.4 times that for Py-1 (0.70 $\mu m^2/s$). Figure 6A shows the dependence of $\overline{D^*_{out}}$ on the initial H_2O_{tot} content at 800 °C with a simple fit by $\overline{D^*_{out}} = A/C_0$, where C_0 is the initial H_2O_{tot} and A is a constant to be determined. The fit is remarkably good except for crystal Py-24. Therefore, an apparent paradox exists: In a single crystal, the apparent diffusivity of the hydrous component is proportional to the OH content (using both profiling and mass-loss methods). For a suite of crystals, the diffusion-out diffusivity is inversely proportional to the initial OH content, which differs from one garnet crystal to another. This paradoxical observation is not due to poor data quality because the experimental data for each crystal are internally consistent. Nor is the observation due to some unknown difference in the two experimental measuring methods because (1) the $\overline{D^*_{out}}$ values obtained from the profiling experiments agree with those obtained from the mass-loss experiments, and (2) the mass-loss experiment Py-7c also shows that D^* is proportional to the OH concentration. To show further that a D^* value that is inversely proportional to OH concentration cannot fit the experimental data, such a profile is calculated and shown in Figure 6B. The calculated profile clearly cannot fit the experimental profiles shown in Figure 2. We conclude that the dependence of the apparent diffusivity of the hydrous component on the crystals used in this study indicates that factors other than OH concen-

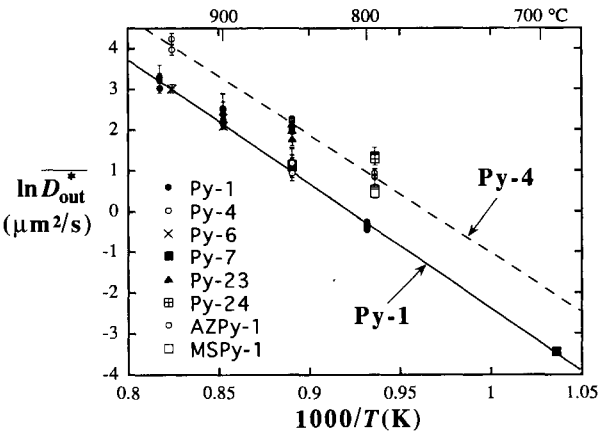

FIGURE 7. Temperature dependence of the diffusion-out diffusivities of the hydrous component in mantle garnet. Error bars are at the 2σ level. (If error bars cannot be seen, they are less than the size of the symbol.) Two lines are least-squares fits to the data for Py-1 and Py-4, respectively.

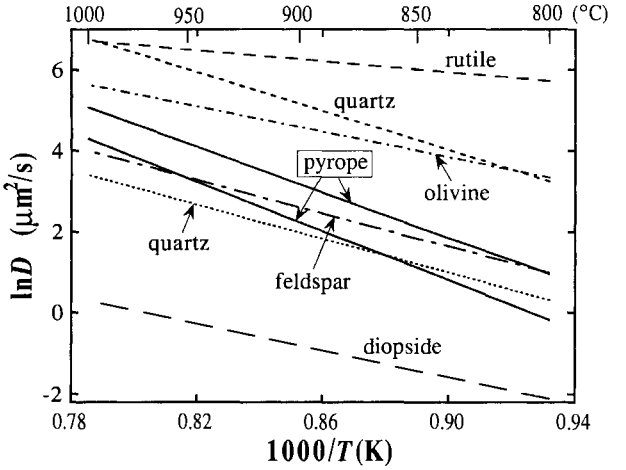

FIGURE 8. Comparison of diffusivities of hydrous component in various minerals. Data are from Kats et al. 1962 (quartz), Johnson et al. 1975 (rutile), Kronenberg et al. 1986 (quartz), Kronenberg et al. 1989 (feldspar), Mackwell and Kohlstedt 1990 (olivine), Ingrin et al. 1995 (diopside), this study (pyrope; diffusion-out diffusivities, Eqs. 6 and 7).

tration also affect the diffusion and incorporation of the hydrous component. There are no significant differences in the compositions of Py-1 and Py-4 (Table 1). Hence, the effects on the apparent diffusivity of the hydrous component are probably due to small variations in Fe^{3+}/Fe^{2+}. This observation places strong constraints on the diffusion and incorporation mechanism of the hydrous component in mantle garnets.

Apparent diffusivities of the hydrous component

All diffusivity values from this study are reported in Table 2 and are shown in Figure 7 in an Arrhenius plot. The $\overline{D^*_{out}}$ values vary from crystal to crystal. Therefore, only data from wafers of the same crystal were used for least-squares fitting with the use of the algorithm of Albarede and Provost (1977) that weights an individual data point according to its error. The $\overline{D^*_{out}}$ values (in squared micrometers per second) of the hydrous component for garnet Py-1 can be described by

$$\ln \overline{D^*_{out}} = (28.20 \pm 1.30) - (30580 \pm 1450)/T \quad (6)$$

and those for Py-4 by

$$\ln \overline{D^*_{out}} = (27.94 \pm 3.27) - (28962 \pm 3812)/T \quad (7)$$

where T is in kelvins. All reported errors are at the 2σ level. The large errors on the preexponential factor and the activation energy in Equations 6 and 7 are highly correlated. Hence, more digits are retained so that the truncation error is negligible in comparison with the $\leq 10\%$ relative error for each $\overline{D^*_{out}}$. The $\overline{D^*_{out}}$ values for crystal Py-4 are ~3 times those for crystal Py-1. The $\overline{D^*_{out}}$ values for other crystals (Table 2, Fig. 7) can be approximated using the inverse proportionality between the $\overline{D^*_{out}}$ values and the initial OH concentrations. The activation energy for the diffusion of hydrous component is 254 ± 12 kJ/mol for Py-1 and 241 ± 32 kJ/mol for Py-4. The two activation energies are in agreement with a weighted average of 253 ± 13 kJ/mol. The activation energy for the apparent diffusivity of the hydrous component is high and similar to that of Fe-Mg exchange and Mg self-diffusion in garnet (Elphick et al. 1985; Cygan and Lasaga 1985; Chakraborty and Ganguly 1991). The D_0^* values can be calculated from the above equations from $\overline{D^*_{out}} = 0.347 D_0^*$.

Diffusion data for hydrous components have been reported for quartz (Kats et al. 1962; Kronenberg et al. 1986), rutile (Johnson et al. 1975), feldspar (Kronenberg et al. 1989), olivine (Mackwell and Kohlstedt 1990), and diopside (Ingrin et al. 1995). These data are compared with our results for pyrope in Figure 8. Although there are large differences in diffusivity values and activation energies, the diffusivities of the hydrous component are all very large (Fig. 8), much larger than those of the other components in crystals. For example, the diffusivities of the hydrous component in mantle garnet during dehydrogenation are at least seven orders of magnitude greater than Fe-Mg interdiffusivity in pyrope (e.g., Elphick et al. 1985), Mg self-diffusivity in pyrope (e.g., Cygan and Lasaga 1985; Chakraborty and Ganguly 1991), and O diffusivity in other silicates (e.g., anorthite, diopside, and olivine) under dry conditions at similar temperatures (e.g., Ryerson et al. 1989; Ryerson and McKeegan 1994).

Geological implications

The experimental dehydrogenation results for mantle garnets demonstrate that significant diffusion can occur within hours at temperatures as low as 800–950 °C. Therefore, a very high cooling rate is necessary to maintain the original OH content of a mantle garnet crystal

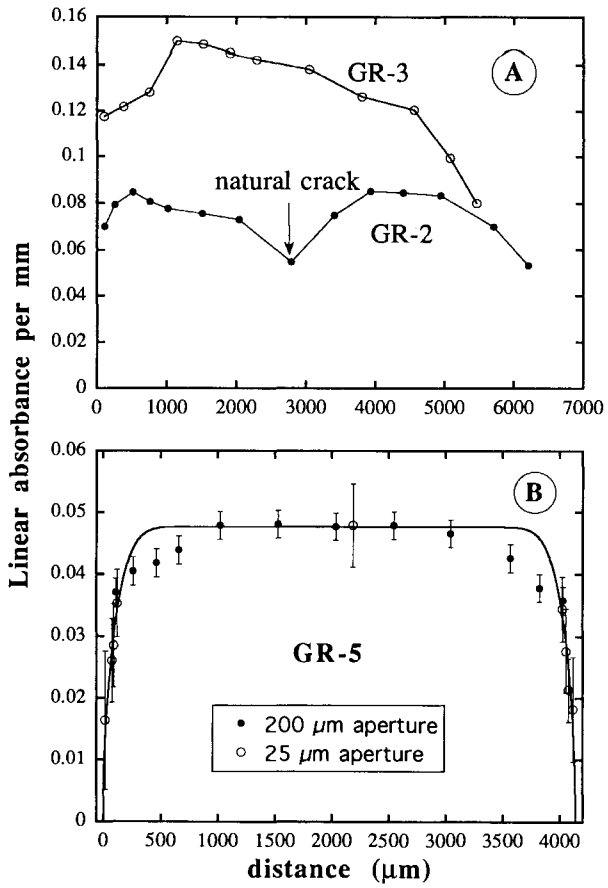

FIGURE 9. Variation of OH concentration (in terms of absorbance of major band per millimeter of sample thickness) vs. distance from one edge to the other for natural mantle-derived pyrope crystals from Garnet Ridge, Arizona. (A) GR-2 (0.432 mm thickness) and GR-3 (0.442 mm). The leftmost and rightmost points are about 150 μm away from the edge. The errors in IR analyses are less than the size of the symbols. (B) GR-5 (0.445 mm thick and 4.14 mm in diameter). The solid curve is the fit assuming that the surface OH content is constant and zero.

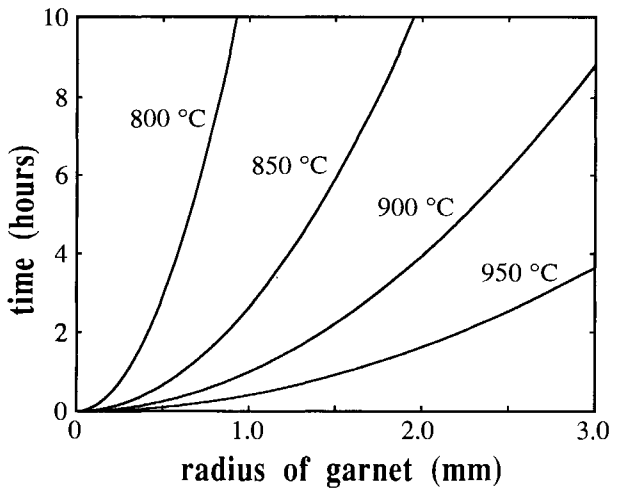

FIGURE 10. Relationship between the size of a pyrope crystal and the time necessary to dehydrogenate 50% of H_2O_{tot} initially present at four temperatures. The diffusion-out diffusivities of Py-1 were used for the calculation.

even in the center of the crystal. Our experimental data can, hence, be used to place constraints on cooling rate and closure temperature and to calculate the time scale required to lose a significant portion of the OH.

The OH zoning profiles were measured for several mantle-derived pyrope crystals (GR-2, GR-3, and GR-5 in Table 1) brought up in the ultramafic diatreme at Garnet Ridge, Arizona. A roughly equidimensional pyrope crystal of 4–6 mm in diameter was cut and doubly polished to obtain a center section of ~0.44 mm thickness. A round aperture of 200 μm was used for the measurement. In one case (GR-5), in which an approximately symmetric profile was obtained, a 25 μm aperture was used to measure the OH concentrations near the edge. The results (Fig. 9) show that OH zoning is common and sometimes complex, and original OH concentration cannot be inferred from some of the profiles (Fig. 9A, GR-2 and GR-3) because there is no plateau region at the center. Although two profiles are asymmetric and complicated by natural cracks and nonsphericity, the OH zonation in one sample (GR-5, Fig. 9B) is roughly symmetric. A large central region has a uniform OH content, and the OH concentration at the surface approaches zero. We therefore attempted a simple model to estimate the cooling time scale assuming that the core OH content had not been disturbed. If the core OH content had been disturbed, the following estimation of the cooling time scale would be a lower limit. According to our diffusion data, the diffusivity is assumed to be $D^* = D_0^* C/C_0$, where D_0^* depends on temperature and hence is a function of time. The diffusion equation can be written as

$$\frac{\partial C}{\partial \tau} = \nabla\left(\frac{C}{C_0}\nabla C\right) \tag{8}$$

where $\tau = \int D_0^*(t)\mathrm{d}t$. The value of τ varies from 0 to τ_∞, where τ_∞ is τ at $t = \infty$ and is a parameter to be fit. The value of τ_∞ is largely dependent on the length of the profile. The initial condition is $C|_{t=0,\, r\le a} = C_0$, where a is the radius of the pyrope. The boundary condition is more difficult to specify because the surface concentration may decrease gradually to zero. In a simple treatment, we used a zero boundary condition: $C|_{r=a,\, t>0} = 0$. The fit of the measured OH profile of GR-5 with the solution of Equation 8 is shown in Figure 9B. Though imperfect, the fit captures the essence of the profile. The best-fit τ_∞ value is 13000 μm^2 with an uncertainty of a factor of 3. To infer the cooling time scale, a functional form of the thermal history must be given so that τ_∞ can be expressed as a function of cooling rate or cooling time scale. An asymptotic cooling model is assumed with $T = T_0/(1 + t/t_c)$ (Eq. 13a in Zhang 1994, with $T_\infty = 0$ K), where T_0 is

the initial T and t_c is the cooling time scale. From the Arrhenius relation for D_0^*, we then have $D_0^*(t) = D_0^*(0)e^{-t/t_d}$, where $D_0^*(0)$ is D_0^* at $t = 0$ ($T = T_0$). The parameter $t_d = t_c(RT_0/E_a)$, where R is the gas constant and E_a is the activation energy, is a time scale for D_0^* to decrease to D_0^*/e. Using the expression for $D_0^*(t)$, we integrated $\int D_0^*(t)dt$ from $t = 0$ to $t = \infty$, which yielded $\tau_\infty = D_0^*(0)t_d$. Therefore, from the best-fit τ_∞ value, t_d and hence t_c can be calculated for a given $D_0^*(0)$ (a function of T_0). Because the initial OH content in GR-5 is close to that in Py-4, Equation 7 was used to calculate D_0^*. If $T_0 = 900$ °C, $D_0^*(0) = 74$ $\mu m^2/s$, $t_d = 174$ s, and $t_c = 1.2$ h. If $T_0 = 1000$ °C, $t_c = 0.16$ h. If $T_0 = 800$ °C, $t_c = 13$ h. If T_0 is as low as 600 °C (Hunter and Smith 1981), the cooling time scale is 0.9 yr. Therefore, the profile indicates a relatively short cooling time scale. This cooling time scale could reflect a combination of the time for the garnet crystal to ascend to the surface with its host and the quench time scale at the surface. The above cooling time scales are similar to that of a mantle xenolith in South Africa with a calculated ascending velocity of ≤ 1 km/h (Ganguly et al. 1995). The flat profile near the center probably represents conditions in the source region.

Examination of Figure 9B shows that part of the profile is not well fit, suggesting that the OH concentration at the surface was not constant. More realistic modeling of the profile requires an assumption about how the surface concentration decreased to zero. Therefore, the OH profile, in principle, stores information on the changing environmental conditions that affect the surface concentration of OH.

Mantle garnets from other environments may be brought up at a slower rate, or the initial temperatures in the mantle may be high. We calculated the time needed for a spherical garnet crystal to lose 50% H_2O_{tot} from the whole crystal by means of Equation 6.22 in Crank (1975). The diffusivities are from Equation 6 for Py-1. The results are shown in Figure 10. At 900 °C, a pyrope crystal with a radius of 1 mm can lose 50% of its bulk H_2O_{tot} in <1 h, and the concentration at the center can be lowered by 20% in 2 h. Therefore, garnet crystals brought up slowly or from a source region with high temperature may not preserve their mantle values of OH contents.

Acknowledgments

We thank G.E. Harlow of the American Museum of Natural History in New York City and the Mineralogical Collection of the University of Michigan for providing some of the samples used in this study, and the Navajo Nation for permission to collect samples on their land. We thank D.R. Bell, J. Ganguly, and C.A. Geiger for their constructive reviews, and S. Dunn, S.C. Semken, and A. Zaman for their help in the field. L.W. thanks J. Windak for helping him to master the FTIR, and C.B. Henderson and P. Tropper for helping with microprobe analyses. This study was supported by a Rackham Faculty Grant, NSF grants EAR-9304161, EAR-9315918, and EAR-9458368 (to Y.Z.), the Scott Turner Award of the University of Michigan, and a grant from the Geological Society of America (to L.W.).

References cited

Aines, R.D., and Rossman, G.R. (1984a) Water content of mantle garnets. Geology, 12, 720–723.

——— (1984b) The hydrous component in garnets: Pyralspites. American Mineralogist, 69, 1116–1126.

Albarede, F., and Provost, A. (1977) Petrological and geochemical mass-balance equations: An algorithm for least-square fitting and general error analysis. Computers and Geosciences, 3, 309–326.

Bell, D.R. (1993) Hydroxyl in mantle minerals. Ph.D. thesis, California Institute of Technology, Pasadena, California.

Bell, D.R., and Rossman, G.R. (1992a) The distribution of hydroxyl in garnets from the subcontinental mantle of southern Africa. Contributions to Mineralogy and Petrology, 111, 161–178.

——— (1992b) Water in Earth's mantle: The role of nominally anhydrous minerals. Science, 255, 1391–1397.

Bell, D.R., Ihinger, P.D., and Rossman, G.R. (1995) Quantitative analysis of trace OH in garnet and pyroxenes. American Mineralogist, 80, 465–474.

Chakraborty, S., and Ganguly, J. (1991) Compositional zoning and cation diffusion in garnets. In Advances in Physical Geochemistry, 8, 120–175.

Crank, J. (1975) The mathematics of diffusion, 414 p. Clarendon, Oxford, U.K.

Cygan, R.T., and Lasaga, A.C. (1985) Self-diffusion of magnesium in garnet at 750–900 °C. American Journal of Science, 285, 328–350.

Doremus, R.H. (1969) The diffusion of water in fused silica. In J.W. Mitchell, R.C. Devries, R.W. Roberts, and P. Cannon, Eds., Reactivity of solids, p. 667–673. Wiley, New York.

Elphick, S.C., Ganguly, J., and Loomis, T.P. (1985) Experimental determination of cation diffusivities in aluminosilicate garnets: I. Experimental methods and interdiffusion data. Contributions to Mineralogy and Petrology, 90, 36–44.

Ganguly, J., Singh, R.N., and Ramana, D.V. (1995) Thermal perturbation during charnockitization and granulite facies metamorphism in southern India. Journal of Metamorphic Geology, 13, 419–430.

Hunter, W.C., and Smith, D. (1981) Garnet peridotite from Colorado Plateau ultramafic diatremes: Hydrates, carbonates, and comparative geothermometry. Contributions to Mineralalogy and Petrology, 76, 312–320.

Ingrin, J., Hercule, S., and Charton, T. (1995) Diffusion of hydrogen in diopside: Results of dehydration experiments. Journal of Geophysical Research, 100, 15489–15499.

Jackson, M.J., and Pollack, H.N. (1987) Mantle devolatization and convection: Implications for the thermal history of the Earth. Geophysical Research Letters, 14, 737–740.

Jambon, A., Zhang, Y., and Stolper, E.M. (1992) Experimental dehydration of natural obsidian and estimation of D_{H_2O} at low water contents. Geochimica et Cosmochimica Acta, 56, 2931–2935.

Johnson, O.W., Deford, J.W., and Paek, S.-H. (1975) Concentration dependent diffusion of H^+ in TiO_2: Analysis of electronic effects in ionic diffusion. Materials Science Research, 9, 253–267.

Kats, A., Haven, Y., and Stevels, J.M. (1962) Hydroxyl groups in α-quartz. Physics and Chemistry of Glasses, 3, 69–75.

Kronenberg, A.K., Kirby, S.H., Aines, R.D., and Rossman, G.R. (1986) Solubility and diffusional uptake of hydrogen in quartz at high water pressures: Implications for hydrolytic weakening. Journal of Geophysical Research, 91, 12723–12744.

Kronenberg, A.K., Rossman, G.R., Yund, R.A., and Huffman, A.R. (1989) Stationary and mobile hydrogen defects in potassium feldspar. Eos, 70, 1406.

Mackwell, S.J., Kohlstedt, D.L., and Paterson, M.S. (1985) The role of water in the deformation of olivine single crystals. Journal of Geophysical Research, 90, 11319–11333.

Mackwell, S.J., and Kohlstedt, D.J. (1990) Diffusion of hydrogen in olivine: Implications for water in the mantle. Journal of Geophysical Research, 95, 5079–5088.

Moulson, A.J., and Roberts, J.P. (1961) Water in silica glass. Transactions of the Faraday Society, 57, 1208–1216.

Ringwood, A.E. (1991) Phase transformations and their bearing on the constitution and dynamics of the mantle. Geochimica et Cosmochimica Acta, 55, 2083–2110.

Rossman, G.R. (1988) Vibrational spectroscopy of hydrous components. In Mineralogical Society of America Reviews in Mineralogy, 18, 193–206.

Rossman, G.R., and Smyth, J.R. (1990) Hydroxyl contents of accessory minerals in mantle eclogites and related rocks. American Mineralogist, 75, 775–780.

Ryerson, F.J., Durham, W.B., Cherniak, D.J., and Lanford, W.A. (1989) Oxygen diffusion in olivine: Effect of oxygen fugacity and implications for creep. Journal of Geophysical Research, 94, 4105–4118.

Ryerson, F.J., and McKeegan, K.D. (1994) Determination of oxygen self-diffusion in åkermanite, anorthite, diopside, and spinel: Implications for oxygen isotopic anomalies and the thermal histories of Ca-Al-rich inclusions. Geochimica et Cosmochimica Acta, 58, 3713–3734.

Wilkins, R.W.T., and Sabine, W. (1973) Water content of some nominally anhydrous silicates. American Mineralogist, 58, 508–516.

Wyllie, P.J. (1979) Magmas and volatile components. American Mineralogist, 64, 469–500.

Zhang, Y. (1994) Reaction kinetics, geospeedometry, and relaxation theory. Earth and Planetary Science Letters, 122, 373–391.

Zhang, Y., Walker, D., and Lesher, C.E. (1989) Diffusive crystal dissolution. Contributions to Mineralogy and Petrology, 102, 492–513.

Zhang, Y., and Stolper, E.M. (1991) Water diffusion in basaltic melts. Nature, 351, 306–309.

Zhang, Y., Stolper, E.M., and Wasserburg, G.J. (1991a) Diffusion of water in rhyolitic glasses. Geochimica et Cosmochimica Acta, 55, 441–456.

——— (1991b) Diffusion of a multi-species component and its role in the diffusion of water and oxygen in silicates. Earth and Planetary Science Letters, 103, 228–240.

Manuscript received June 16, 1995
Manuscript accepted January 26, 1996